Composite Structures 389 (2026) 120440

Contents lists available at ScienceDirect

Composite Structures

journal homepage: www.elsevier.com/locate/compstruct

Fracture process zone and crack migration in pure mode II bonded composite joints: influence of pre-crack, stacking sequence, normalized crack-geometry

Ishan Manoj *, Daniel Bernardes de Castro, John-Alan Pascoe, René Alderliesten

Aerospace Structure and Materials, Delft University of Technology, 2600 GB Delft, the Netherlands

ARTICLE INFO

Keywords:
Fracture toughness
Stacking sequence
Pre-cracking
Damage evolution
Apparent crack length
Digital image correlation
Finite element analysis

ABSTRACT

This study examines how loading mode during pre-cracking, stacking sequence, and initial delamination ratio (a_0/L) influence Mode II fracture characterization (G_{IIC}) of bonded composite joints. 3-point End-Notched Flexural tests were performed on Unidirectional (UD) and Quasi-Isotropic (QI) carbon fibre/epoxy laminates bonded with AF163-2 K adhesive. Results reveal that fracture toughness and crack migration are governed by the morphology of the Fracture Process Zone (FPZ).

In UD laminates, Mode I pre-cracking forms localized FPZ, requiring intense plastic deformation to transition into shear-dominated FPZ, capturing the upper-bound fracture resistance. Conversely, Mode II pre-cracked specimens exhibited diffused shear FPZ, resulting in lower G_{IIC}.

In QI laminates, diffused FPZ by Mode II pre-cracking delays crack migration into the weaker interlaminar, promoting growth within the bond-layer. However, localized FPZ from Mode I pre-cracks requires intense plastic deformation and shear cracks for the crack to grow in the bond-layer, triggering earlier migration. The crack migration was sensitive to the "a_0/L" *ratio*: a ratio of 0.4 induces independent interlaminar delamination, while 0.6 displays angular crack-migration. These mechanisms remained invariant when the span-length was scaled, provided the normalized crack length was preserved.

This study demonstrates that G_{IIC} is process-dependent, underscoring the need to characterize fractures based on FPZ evolution.

1. Introduction

Adhesively bonded composite joints are widely employed in structural applications due to their ability to reduce structural weight, provide better stress distribution, and cause less damage to the adherends compared to drilling holes for fasteners [1–3]. In practical applications, load transfer between substrates occurs through a combination of loading modes [4–6]. However, adhesively bonded joints are designed to maximize in-plane shear loading, promoting crack propagation in a constrained manner parallel to the bonded interface through a sufficient overlap length [7,8]. Nevertheless, the fracture characterization of bonded joints under pure Mode II loading remains complicated due to the sizeable fracture process zone (FPZ) formed ahead of the crack tip, challenges in crack tip identification, and the tendency of crack migration from the bond layer to the interlaminar region of composites [9,10]. These challenges become more complex for toughened structural adhesive joints due to the extensive plastic deformation that influences the process zone [11,12]. Hence, a detailed understanding of Mode II fracture characterization is crucial for designing bonded composite structures with enhanced damage tolerance [13].

While ASTM [14] and ISO [15] standards provide well-established guidelines for Mode II delamination characterization in unidirectional (UD) fiber-reinforced composites, no standardized procedures currently exist for adhesively bonded joints [16,17]. Although researchers use established methods for Mode I adhesive fracture (e.g., DCB approaches based on ISO 25217:2009 [18]) and cleavage testing, they have not yet established a universally accepted standard equivalent to ENF for pure Mode II adhesive fracture. While ASTM and ISO standards provide well-established guidelines for Mode II delamination characterization in unidirectional (UD) composites, researchers still lack standardized procedures for Mode II fracture characterization of adhesively bonded joints. This is primarily due to the fundamental differences in fracture

* Corresponding author.
E-mail address: i.manoj@tudelft.nl (I. Manoj).

https://doi.org/10.1016/j.compstruct.2026.120440
Received 26 January 2026; Received in revised form 29 April 2026; Accepted 9 May 2026
Available online 10 May 2026

mechanisms: unlike UD laminates, adhesively bonded interfaces, particularly those involving toughened structural adhesives, exhibit extended FPZs and pronounced nonlinear deformation. As a result, the direct application of Mode II delamination protocols to bonded joints can lead to ambiguities in crack-tip identification and in the interpretation of fracture energy, especially for relatively thick or ductile adhesive layers.

This gap has resulted in significant variation in the reported critical strain energy release rate (G_{IIC}) values for the same adhesive system. For instance, the structural adhesive AF163-2 K has been reported to have mode II fracture toughness values varying by more than an order of magnitude, ranging from 0.67 N/mm to 17.8 N/mm [11,12,19–24]. Hence, there is a significant gap in the literature regarding the poor reproducibility of fracture toughness and the factors that influence it. Several studies have demonstrated the role of the FPZ size and morphology in governing fracture response, particularly in pure Mode II, where shear-dominated loading extends significantly ahead of the crack tip [25–27]. This highlights that process parameters, including FPZ evolution, the stability of crack growth, and the interaction between the adherend and adhesive, significantly influence the variability of Mode II fracture resistance [28–30]. It underscores that the factors that can dictate the evolution of FPZ and crack migration in adhesively bonded composite joints remain insufficiently understood [31–34].

For example, standard protocols [35–37] allow for pre-cracking in either Mode I or Mode II to initiate a pre-crack for fracture characterization under pure Mode II loading. Typically, a pre-crack is employed to ensure crack growth stability. However, Mode II fracture resistance can also be influenced by the initial pre-cracking mode, which can affect the formation of the initial FPZ and its subsequent evolution under Mode II loading [38–40]. Despite the potential of the pre-cracking mode to fundamentally alter the measured fracture resistance, this aspect has received limited attention. Furthermore, disbond growth and delamination in adhesively bonded composite joints are strongly influenced by the stacking sequence of the adherends [13,41–44]. In unidirectional laminates, crack growth is often constrained within the adhesive layer, whereas in quasi-isotropic (QI) laminates, competition between adhesive fracture and interlaminar delamination can lead to crack migration. The extent to which the pre-cracking mode interacts with laminate architecture to influence FPZ development, crack migration, and the resulting G_{IIC} remains largely unexplored. Additionally, although geometric parameters such as the initial delamination ratio (a_0/L) are known to influence compliance and stability in Mode II tests, their role in governing fracture mechanisms, FPZ evolution, and crack migration in bonded composite joints remains unclear.

The objective of the present study is to systematically investigate the influence of pre-cracking mode (Mode I versus Mode II), stacking sequence (UD versus QI), and initial delamination ratio (a_0/L) on Mode II fracture behavior of adhesively bonded composite joints. Three-point End-notched flexural bending (ENF) (Fig. 1) tests are conducted using a toughened structural film adhesive (AF163-2 K), with particular emphasis on FPZ morphology, crack migration behavior, and process-dependent fracture resistance. This work demonstrates that the measured G_{IIC} is inherently process-dependent rather than a unique material constant, as elucidated by the mechanisms governing the evolution of FPZ and the stability of the crack path. Mixed-mode fracture behavior is commonly characterized using the Mixed-Mode Bending (MMB) test, which enables controlled mode-mixity and the development of fracture envelopes. However, the present study focuses specifically on pure Mode II fracture behavior; therefore, ENF testing is employed to isolate shear-dominated mechanisms and enable a clearer interpretation of FPZ evolution and crack migration. The findings offer valuable insights for interpreting Mode II fracture data and developing more physically driven fracture characterization approaches for adhesively bonded composite structures.

2. Experiments

2.1. Materials and manufacturing

Two different batches of UD and QI laminates were manufactured by sequentially stacking the plies of HexPly IM7/8552 carbon fibre/epoxy prepreg, with a nominal fiber volume fraction of 57.70%, supplied by Hexcel (as indicated in the data sheet) [45]. The laminates were manufactured using the hand lay-up process, with vacuum debulking applied after each alternate ply. The length of the adherend was 250 mm, and its width was 25 mm. The laminates were cured in an autoclave according to the manufacturer's recommendation at an absolute pressure of 7 bar and a maximum temperature of 180 °C for 7 h [45].

After post-curing, an ultrasound C-scan was performed on the laminate to verify the quality of the manufactured composite. The pulse-echo C-scan (see representative scan in Fig. 2b) shows a consistent signal across the laminate width. The lack of 'red' or 'orange' zones (which indicate too much signal attenuation associated with voids or delamination) confirms the absence of macro-voids or pre-existing delamination that could lead to premature failure or misleading G_{IIC} values. The 7-bar autoclave cycle at 180ºC was effective in achieving high consolidation. The C-scan results were further corroborated by visual inspections of the cut specimen edges, which showed a clean bond-line and no interlaminar defects.

The top and bottom adherends of the ENF specimens were cut from the laminate using an ACS 600 comp-cut cutting machine using a cutting disc and water as a coolant, before being bonded together. The thickness of the UD laminate was determined by averaging 5 points on each side: $t = 2.16 \pm 0.09$ mm. The surface of the composites was carefully abraded

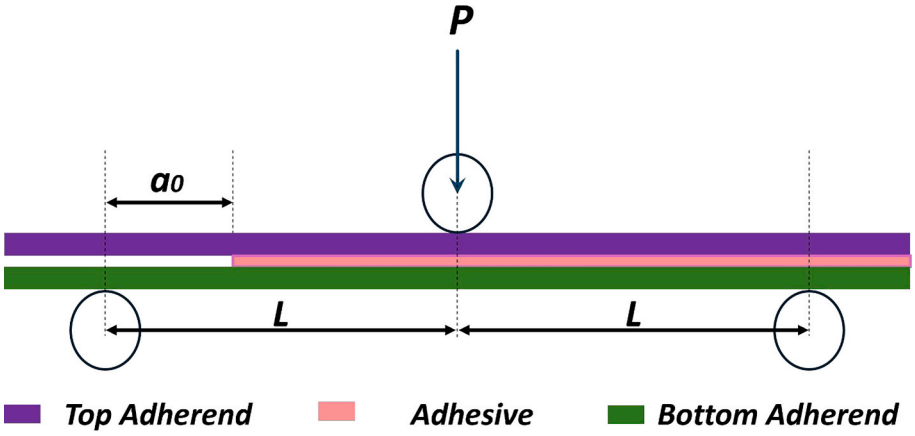

Fig. 1. Schematic representation of 3-point bending End-Notched Flexural Test.

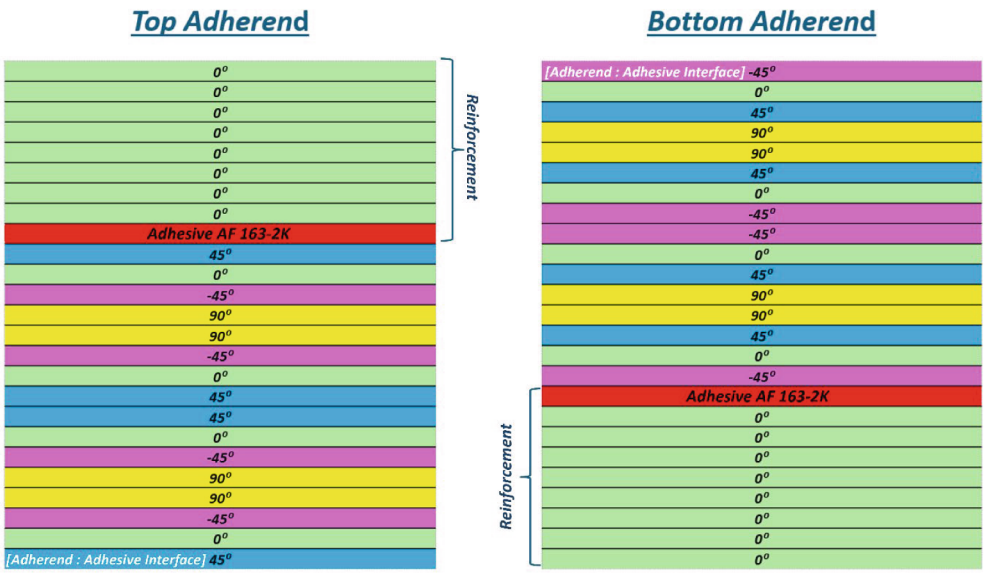

a

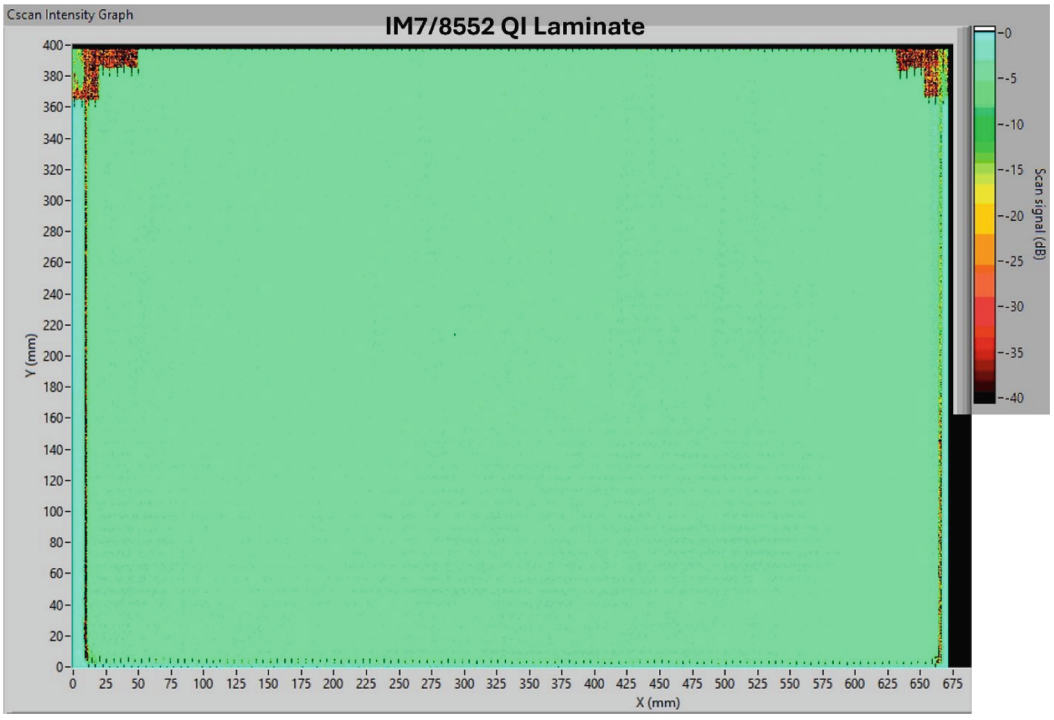

b

Fig. 2. (a) The lay-up sequence for Quasi-Isotropic (QI) laminates reinforced with eight unidirectional (UD) lamina and an additional adhesive layer. (b) A C-scan was performed after the manufacturing of the composite laminate to ensure the quality of the manufactured CFRP.

using fine-grit sandpaper (P120) along the fiber direction. The surface was then cleaned with a fresh cotton cloth soaked in isopropanol. The structural film adhesive AF163-2 K was used to bond the adherends and was supplied by 3 M. An initial crack of 70 mm was created in ENF specimens using a very thin (≈ 0.1 mm) Teflon insert. The thickness of the Teflon insert was used only to introduce the initial pre-crack and does not define the final adhesive layer thickness.

The top and bottom adherends of the bonded ENF assembly were again autoclaved according to the manufacturer's curing recommendation at a differential pressure of 3.5 bar and a maximum temperature of 130 °C for 2 h [46]. The bonded composite laminates were then precisely cut to the required specimen geometry. The thickness of the adhesive layer after curing was measured using an optical microscope, which was 0.17 ± 0.02 mm. This difference arises from adhesive flow and squeeze-out during bonding and curing. The layup of QI laminates is shown in Fig. 2a.

The specimen configuration was designed with the following rationale:

- *Reduction of Decoupling Moments:* The specimen configuration was intentionally designed to promote a controlled Mode II-dominated fracture response while minimizing undesired coupling effects that could otherwise interfere with the crack migration analysis. To achieve this, QI adherends were tailored so that the bonding interface lies between −45° and + 45° plies, which favors shear-dominated deformation at the crack tip. In addition, the stacking sequences of the top adherend of QI adherend was manufactured using a stacking sequence ([45/0/-45/0]s whereas the bottom adherend of QI laminates was manufactured using ([-45/0/45/0]s near the bonded interface to minimize the decoupling moments (Fig. 2a).
- *Global Stiffness Matching:* It was essential to have a direct comparison of fracture behavior across different stacking sequences without results being influenced by unintended stiffness mismatches. The additional UD plies and adhesive layer (the 'reinforcement' seen in Fig. 2a) were added away from the bond line to ensure the global bending stiffness of the QI specimens matched that of the UD specimens.
- *Focus on Crack Migration:* The primary objective of this specific configuration was to investigate the competition between disbond failure and interlaminar delamination. By strategically placing the adhesively bonded interface between 45° and −45° layers of both QI laminates, we could systematically observe how the FPZ morphology influences the 'survival time' of the crack within the adhesive before it migrates into the substrate.

The final thickness of a single adherend with reinforced adhesive and plies was ≈ 3.4 ± 0.05 mm. A minimum of three valid specimens were tested for each configuration to ensure statistical repeatability. In several cases, additional specimens were tested to further confirm the consistency of the observed crack migration behavior. A total of 22 valid specimens were tested in the present study. All reported G_{IIC} values and peak loads include the corresponding standard deviations to quantify the experimental scatter and ensure the reliability of the observed trends.

2.2. Test Set-Up

The ENF tests were performed on a Zwick static testing machine equipped with a 10 kN load cell. The tests were conducted in a displacement-controlled setup with a quasi-static rate of 0.5 mm/min. The test setup for the ENF tests is depicted in Fig. 3. A high-resolution camera was equipped on one side to track the propagation of the crack (Camera). One lateral side of the specimens was painted white, and then, using a sharp knife with a ≈ 0.1 mm nib, marks were made at regular intervals of 1 mm. Similarly, a high-resolution Digital Image Correlation (DIC) camera was used to monitor changes in the speckle pattern from the other side. The DIC helped obtain a full-field strain field and a displacement map, while the rear camera provided complementary visual crack tracking, enabling accurate measurement of disbond growth. Very fine speckles were applied to specimens on the DIC camera's side to form trackable patterns.

Under the 3-point bending ENF configuration, the stress state is dominated by in-plane shear, and out-of-plane displacements are negligible for the purposes of observing crack path stability. The primary objective of the DIC analysis was to characterize the FPZ morphology and track crack migration within the bond line and interlaminar interfaces.

The second camera was positioned on the rear side of the specimen to monitor real-time crack growth. This camera was synchronized with the DIC system and the load-cell controller, enabling correlation between the observed crack-front evolution and the measured strain fields. Using a single-camera setup enabled higher magnification of the bond-layer interface, which was critical for capturing the transition from localized to diffused FPZ morphology, as described in the results. While a stereo (3D) DIC system could provide out-of-plane displacement information, it was not deemed necessary for the objectives of this study, which focus on crack migration mechanisms and FPZ development under predominantly in-plane loading conditions.

Pictures for crack tracking and DIC were taken at an interval of 2 s. Sufficient light sources were used to illuminate the test environment, reducing the scatter of outside lighting. All tests were conducted under laboratory conditions at 22 °C and 60% relative humidity.

2.2.1. Pre-cracking, geometric details, and initial delamination ratio

ENF specimens were prepared to introduce mode I and mode II pre-cracks separately. The span length between the two bottom rollers is denoted as "*2L*", in accordance with ASTM D7905 [14], where a distance "*L*" is maintained between the consecutive rollers. The initial crack length, a_0, is measured from the first bottom roller to the crack tip. Mode II pre-cracking was conducted at a loading rate of 0.5 mm/min, followed by unloading at a rate of 5 mm/min. The test was stopped when the vertical lines made on top and bottom adhered, showing a shift within the range of 2–5 mm. For Mode I pre-cracking, both adherends of the specimen were pulled in tension, producing a sharp pre-crack of 2.5 ±

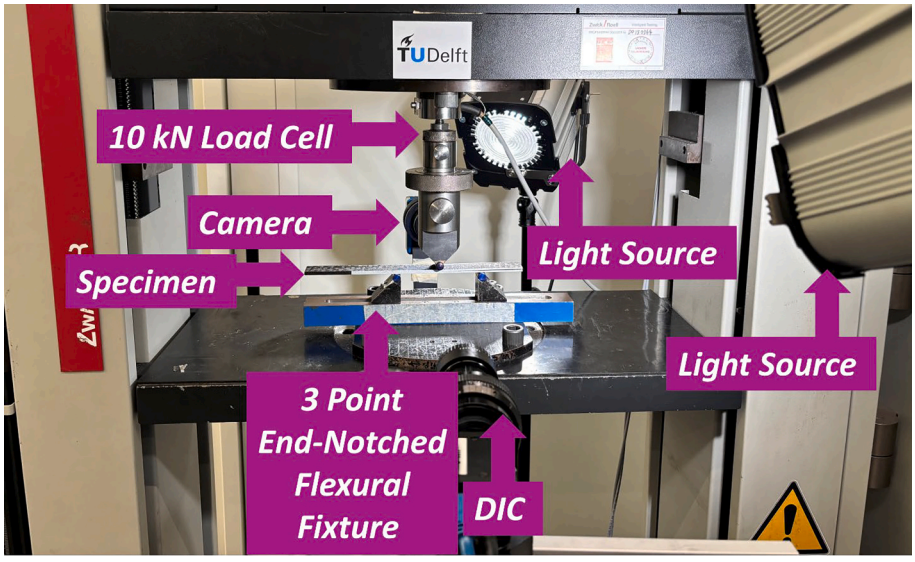

Fig. 3. Quasi-static ENF test being conducted in the laboratory using a Zwick Universal testing machine. DIC, Camera, and light source are illustrated in the image.

0.5 mm. An illustration of the ENF sample tested is shown in Fig. 1. The different ENF configurations tested are summarized in Table 1.

2.3. Data reduction schemes

Several data reduction schemes in the literature calculate the fracture resistance from experimental data of ENF specimens [47,48]. Classical approaches, such as the Compliance Calibration Method (CCM) and Corrected Beam Theory (CBT), rely on the real-time, accurate measurement of the physical crack length during propagation. However, these methods are susceptible to experimental error and subjective interpretation, as identifying the precise location of the crack tip under Mode II loading is inherently difficult [49,50]. This challenge is further exacerbated by the development of large FPZs, which are only marginally captured by conventional CCM or CBT methods [16,17,51].

Given that the focus of the present work is the evolution of the FPZ and crack migration rather than a comparison of data reduction methodologies, the Compliance-Based Beam Method (CBBM) proposed by De Moura et al. [52,53] was exclusively utilized. The CBBM is widely regarded as a robust and reliable scheme because it circumvents the need for direct crack length monitoring [42,43,54–56]. While the authors conducted a comprehensive comparison of multiple data reduction schemes in a separate study, identifying the CBBM as the most accurate and consistent approach, the present work focuses exclusively on the physical mechanisms of FPZ evolution and crack migration.

CBBM employs an equivalent crack length (a_f), often referred to as the apparent crack length, which is derived directly from the specimen's compliance. Crucially, this equivalent crack length accounts for the energy dissipated within the FPZ, effectively capturing the effects of plasticity and micro-damage ahead of the physical crack tip. The CBBM utilizes an apparent flexural modulus (E_{1f}) calculated from the initial experimental compliance (C_0). C_C is corrected experimental compliance adjusted to account for the shear deformation of the adherends. C_{0C} initial corrected compliance at the start of the test, similarly corrected for shear effects, is used to calculate the apparent flexural modulus (E_{1f}). This approach enables the method to account for inherent variability in material properties and specimen conditions, providing a more physically consistent evaluation of G_{IIC} in the presence of extensive process zone development. Equation (1) to (5) how to obtain G_{IIC} as proposed by De Moura et al. for the CBBM [52]. This data reduction scheme relies upon measurement of force (P), displacement (δ), compliance (C), width of specimen (B), thickness of each arm (h), half-span length (L), interlaminar shear modulus (G_{13}), and initial crack length (a_0).

$$E_{1f} = \frac{3a_0^3 + 2L^3}{8Bh^3C_{0C}} \tag{1}$$

$$C_C = C - \frac{3L}{10G_{13}Bh} \tag{2}$$

$$C_{0C} = C_0 - \frac{3L}{10G_{13}Bh} \tag{3}$$

$$a_f = \left[\frac{C_C}{C_{0C}}a_0^3 + \left(\frac{C_C}{C_{0C}} - 1\right)\frac{2L^3}{3}\right]^{\frac{1}{3}} \tag{4}$$

Table 1
List of ENF samples tested with different layups, normalized geometry, and specimen number.

Lay-Up	*Pre-Cracking Mode*	*"a_0" [mm]*	*L [mm]*	*"a_0/L"*	*Specimens*
UD	Mode I	30	50	0.6	6
	Mode II	30	50	0.6	3
QI	Mode I	30	50	0.6	3
	Mode II	30	50	0.6	4
	Mode II	20	50	0.4	3
	Mode II	42	70	0.6	3

$$G_{IIC} = \frac{9P^2a_f^2Coc}{2B\left(3a_0^3 + 2L^3\right)} \tag{5}$$

3. Results and Discussions

The discussion is structured first to elucidate the influence of the pre-cracking mode (Mode I vs. Mode II) on the fracture resistance of UD and QI bonded laminates. This analysis explicitly correlates the observed fracture toughness with the mechanisms of crack migration as dictated by the laminate stacking sequence. Following this, the investigation explores the influence of the initial delamination ratio (a_0/L), examining its interplay with the span length and its role in governing the stability of the crack path. The relationship between process zone evolution and global fracture response is established by synthesizing these observations.

3.1. Mode I vs. Mode II Pre-cracking: UD ($a_0/L = 0.6$)

All the UD ENF specimens exhibited stable crack growth, displaying cohesive failure in the bond layer. The force–displacement curve of the UD ENF specimens is shown in Fig. 4. The peak load exhibited excellent repeatability, with an average value of 2868 ± 134 N in Mode I pre-cracked ENF specimens. The mode II pre-cracked ENF specimens displayed a peak load of 3240.66 ± 161.2 N. The nonlinear portion of the load–displacement curve in the Mode I pre-cracked UD ENF specimens showed pronounced plasticity. This behavior signifies that Mode I pre-cracking produces a relatively minor FPZ ahead of the crack tip, which in turn promotes localized plastic deformation during the final fracture stage.

The critical Mode II strain energy release rate (G_{IIC}) was evaluated at the peak force to avoid the parasitic effects of local compression and constraints from the loading indenter, a standard protocol in literature to ensure data integrity [42,43,54,55]. The results revealed a significant disparity in fracture toughness; the G_{IIC} value for Mode I pre-cracked specimens was ≈ 14.67 ± 0.99 N/mm, whereas the Mode II pre-cracked specimens displayed a lower G_{IIC} value of ≈11.85 ± 0.87 N/mm (Fig. 4). The Mode II pre-cracked UD specimens showed a ≈19.22% decrease in fracture toughness compared to Mode I pre-cracking. This supports the conclusion that the broader FPZ in Mode II pre-cracks results in a more conservative, lower-bound toughness estimate. The wide variability in reported G_{IIC} values for the AF163-2 K system is now discussed in the context of process-dependent fracture behavior, providing a basis for interpreting the trends observed in the present work [11,12,19,20,23,24,30].

The underlying mechanism for this difference lies in the evolution of the FPZ within the stable cohesive bond layer. Mode I pre-cracking generates a sharp, singular crack tip with a negligible initial shear-damage zone that must overcome a higher energy barrier to evolve into a shear-dominant FPZ, thereby capturing the upper-bound fracture resistance of the adhesive. Conversely, in Mode II pre-cracked specimens, a shear-driven FPZ is already established (Fig. 5). This pre-existing, diffuse FPZ influences the global stiffness response, resulting in a lower G_{IIC} value. These findings suggest that Mode II pre-cracking provides a more representative, yet conservative, measure of the adhesive's inherent shear resistance by accounting for the pre-established damage zone. The role of the FPZ in governing crack propagation under shear-dominated loading is supported through comparison with existing literature [12,33,34,40,57]. The experimentally observed evolution of an extended FPZ is consistent with prior findings, in which increased damage-zone development influences energy dissipation and fracture resistance [57–59].

3.2. Mode I vs. Mode II pre-cracking: effect of QI lay-up ($a_0/L = 0.6$)

The fracture response of QI specimens also exhibited significant

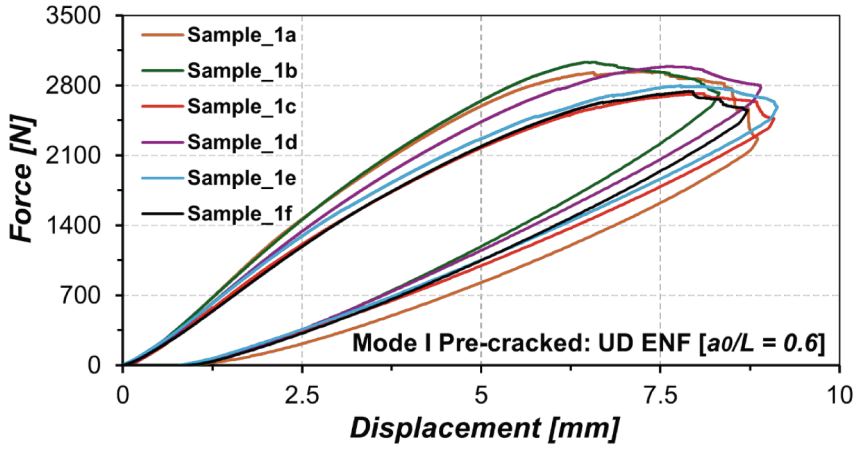

a

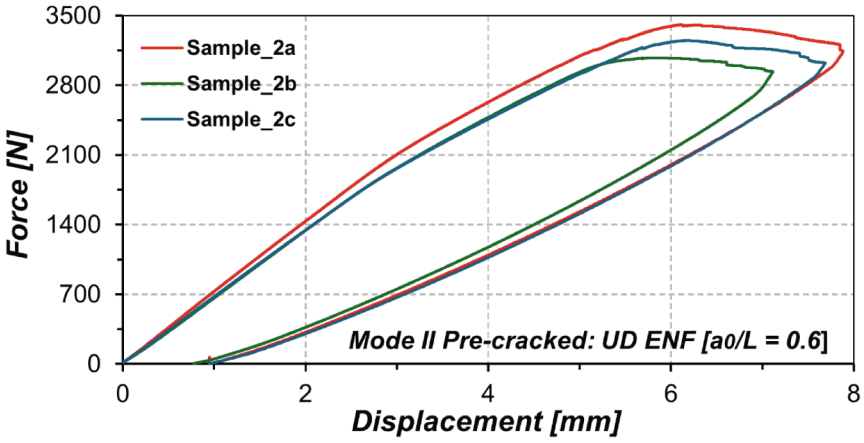

b

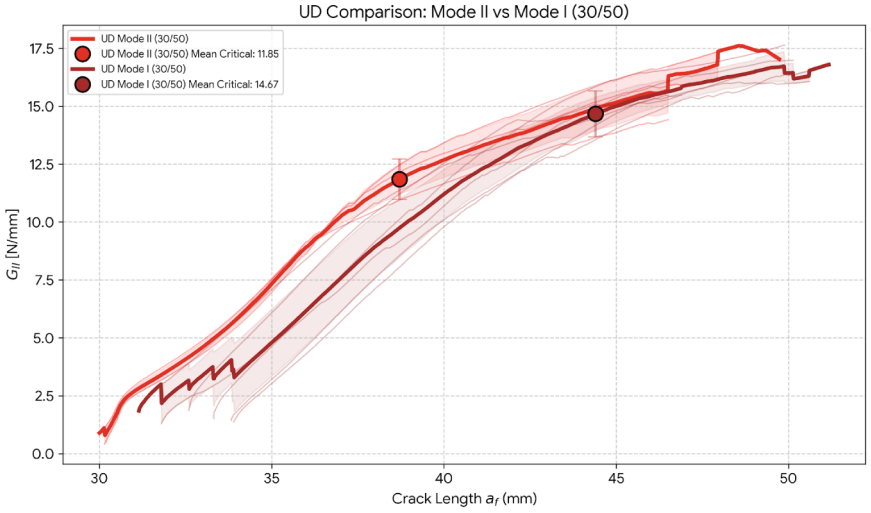

c

Fig. 4. (a) Force-Displacement graph of Mode I pre-cracked ENF UD specimens [$a_0/L = 0.6$; 30/50], (b) Force-Displacement graph of Mode II pre-cracked ENF UD specimens [$a_0/L = 0.6$; 30/50], (c) Variation of SERR vs. crack length for Mode I and Mode II pre-cracked ENF UD specimens [$a_0/L = 0.6$; 30/50].

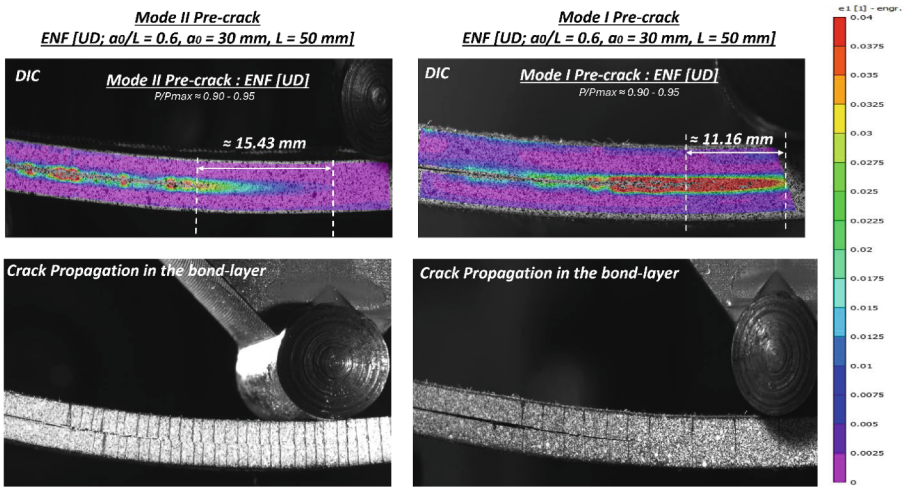

a

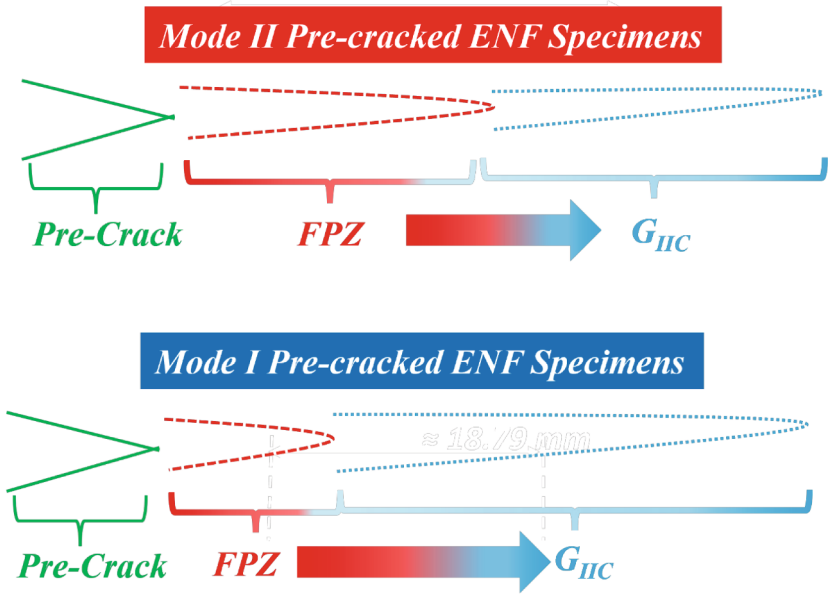

b

Fig. 5. (a) DIC images coupled with regular photographic images before final fracture, showing qualitative comparison of FPZ evolution and morphology for Mode I and Mode II pre-cracked ENF UD specimens [$a_0/L = 0.6$; 30/50]. Images are captured at approximately 90–95% of the critical load to compare the FPZ development at a near-critical state. (b) Schematic representation of shear-driven FPZ that distributes damage ahead of the pre-crack tip, thereby reducing the localized energy release rate at the crack tip and yielding a different fracture toughness estimate.

sensitivity to the pre-cracking history, but diverged from the trends established in the UD specimens. The Mode II pre-cracked QI specimens attained an average maximum load of 4681 ± 353.03 N, corresponding to a mean G_{IIC} of ≈ 9.33 ± 1.24 N/mm. In contrast, the Mode I pre-cracked QI specimen displayed a significantly lower average maximum load of 3999.5 ± 65.29 N and a reduced G_{IIC} of 7.31 ± 0.39 N/mm (Fig. 6). A significant finding is the ≈27.63% increase in G_{IIC} for Mode II pre-cracked QI specimens over Mode I. This statistically confirms the "inversion" trend, in which the diffuse FPZ stabilizes the crack within the adhesive layer for longer than the localized Mode I pre-crack.

Interestingly, the hierarchy of fracture toughness in QI laminates is inverted compared to that of UD laminates. This phenomenon is elucidated by the competitive failure mechanics between the adhesive bond layer and the relatively weak + 45°/0° and −45°/0° interlaminar interface of the QI adherend. In UD laminates, the absence of weak off-axis interfaces constrains the crack to the bond-layer, allowing Mode I pre-cracking to capture an upper-bound toughness through intense localized plasticity. However, in QI laminates, the low interlaminar strength, measured at approximately ≈*1/15th* order of magnitude lower than the adhesive shear strength (see Table 2), introduces a preferred path for crack migration. The observed crack-migration behavior in QI laminates is interpreted in light of established energy-based criteria for crack-path selection. The transition from adhesive failure to interlaminar delamination is consistent with the tendency of cracks to propagate along the path of least resistance, as reported in the literature [60].

The disparity in G_{IIC} values (Table 3) is directly attributable to the extent of stable cohesive growth prior to the onset of migration, which is governed by the morphology of the pre-existing FPZ:

- Mode II Pre-cracking: This mode establishes a broad and diffuse shear-driven FPZ within the adhesive. This pre-developed zone creates a weak region, allowing the crack to propagate more extensively

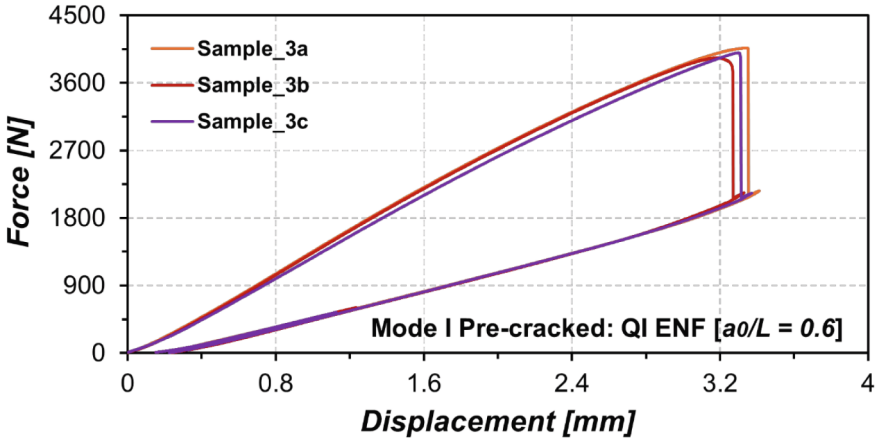

a

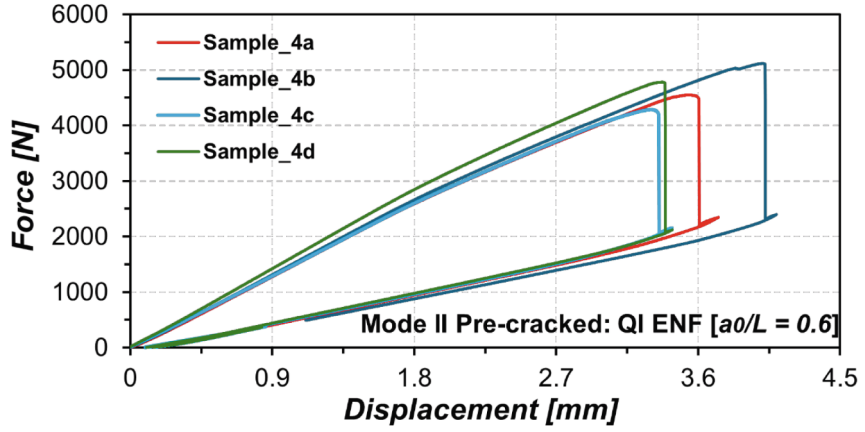

b

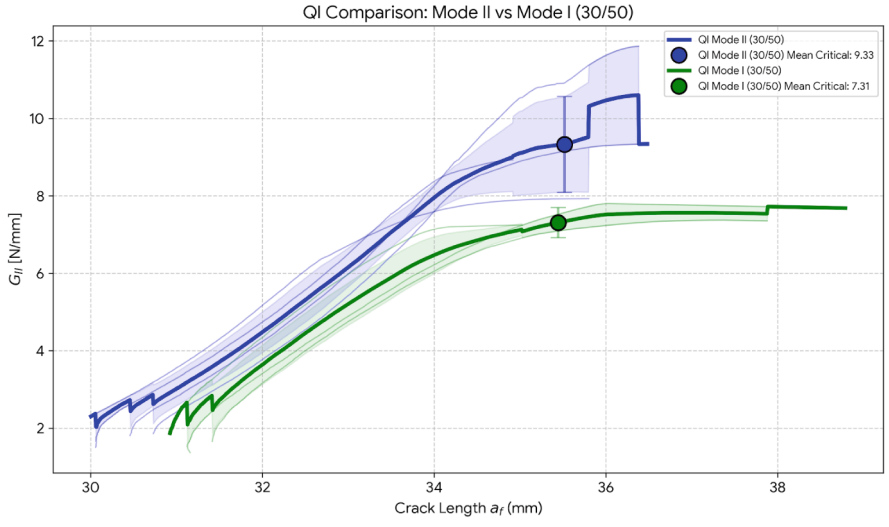

c

Fig. 6. (a) Force-Displacement graph of Mode I pre-cracked ENF QI specimens [a_0/L = 0.6; 30/50], (b) Force-Displacement graph of Mode II pre-cracked ENF QI specimens [a_0/L = 0.6; 30/50], (c) Variation of SERR vs. crack length for Mode I and Mode II pre-cracked ENF QI specimens [a_0/L = 0.6;30/50].

Table 2
Interlaminar Fracture Properties for IM7/8552 vs. Adhesive AF163-2 K [11,12,61,62].

	G_{IC} [N/mm]	G_{IIC} [N/mm]	σ_n [MPa]	σ_t [MPa]
IM7/8552	*0.24*	*0.739*	*80.1*	*97.6*
Adhesive	*3.05*	11.85 ± 0.87	*35*	*35*

Table 3
List of ENF samples tested with different layups, normalized geometry, and G_{IIC} values.

Lay-Up	*Pre-Cracking Mode*	*"a_0" [mm]*	*L [mm]*	*"a_0/L"*	*G_{IIC} [N/mm]*
UD	Mode I	30	50	0.6	14.67 ± 0.99
	Mode II	30	50	0.6	11.85 ± 0.87
QI	Mode I	30	50	0.6	7.31 ± 0.39
	Mode II	30	50	0.6	9.33 ± 1.24
	Mode II	20	50	0.4	11.04 ± 1.3
	Mode II	42	70	0.6	9.41 ± 0.91

within the toughened adhesive layer before the stress field satisfies the criteria for interlaminar delamination. Moreover, an angular migration to crack growth followed by instant failure was observed after crack has propagated considerably in the bond-layer due to large FPZ. The resulting higher G_{IIC} values reflect this prolonged energy dissipation within the bond layer (Fig. 7).

- Mode I pre-cracking: This mode generates a sharp, localized FPZ. The high energy barrier required to transition this localized tip into a shear-dominant crack exceeds the fracture threshold of the + 45°/0° and −45°/0° interface. Consequently, the crack finds a path of least resistance by migrating into the interlaminar region. This early exit from the bond-layer limits the total energy dissipated, leading to the lower observed G_{IIC}.

While UD specimens exhibited consistent stable cohesive failure, all QI specimens eventually transitioned to unstable failure upon crack migration. The failure was stable only as long as the crack remained confined to the bond layer; however, nucleation in the interlaminar region triggered rapid, catastrophic propagation (Fig. 7). These results demonstrate that in complex stacking sequences, the pre-cracking mode dictates the survival time of the crack within the adhesive layer, fundamentally shifting the perceived fracture resistance of the joint.

3.3. Normalized crack length (a_0/L) on damage tolerance

To evaluate the influence of geometric constraints on FPZ development and crack stability, the a_0/L ratio of the QI ENF laminates with mode II pre-crack was reduced from *0.6 to 0.4*. This variation enables an assessment of how the available bond-line length affects the weak interlaminar strength of the substrate. The QI ENF specimens with mode II pre-crack with a shorter a_0/L ratio (*0.4*) exhibited a significantly higher average peak load of 6220.825 ± 265 N, corresponding to a G_{IIC} of 11.04 ± 1.3 N/mm (Fig. 8). This represents a notable increase in fracture energy compared to the $a_0/L = 0.6$ specimens. Reducing the a_0/L ratio from 0.6 to 0.4 resulted in an ≈18.33% increase in apparent fracture energy, despite identical Mode II pre-cracking conditions.

3.3.1. Geometric constraints on FPZ development

The disparity in G_{IIC} values is attributed to the available growth space within the bond layer before the crack tip experiences the compressive stress field and geometric constraints imposed by the central loading roller. In the lower a_0/L specimens, the longer FPZ generated by Mode II pre-cracking has a larger longitudinal distance to evolve within the adhesive layer. This extended propagation path enables greater energy dissipation prior to the onset of angular crack migration to the weak inter-laminar region followed by catastrophic failure, thereby increasing the apparent fracture toughness. The transition in failure mechanism and analysis of crack growth reveals a fundamental shift in failure morphology as a function of the a_0/L ratio.

- Specimen with longer a_0/L (0.6): As demonstrated in Section 3.2, there is a crack migration before the final failure of the specimen, as shown in Fig. 9. This represents a competitive failure between the shear-loaded bond line and the weak composite interface.
- Specimen with shorter a_0/L (0.4): These specimens exhibited a distinctly different mechanism. The crack initially propagated stably within the adhesive layer. However, rather than a gradual angular migration, a sudden two-sided independent delamination occurred within the adherend laminate. Independent delamination means that no crack migration was observed from the bond-layer to adjacent interlaminar interface. This secondary delamination propagated simultaneously ahead of and behind the primary crack tip, leading to immediate catastrophic failure.

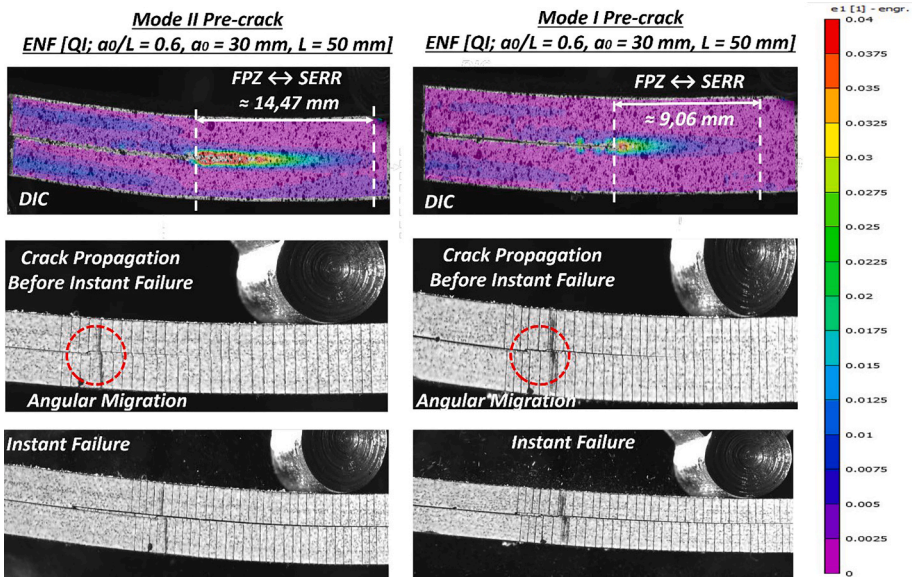

Fig. 7. DIC images coupled with camera car images showing qualitative FPZ evolution and morphology for Mode I and Mode II pre-cracked ENF QI specimens [a_0/L = 0.6; 30/50].

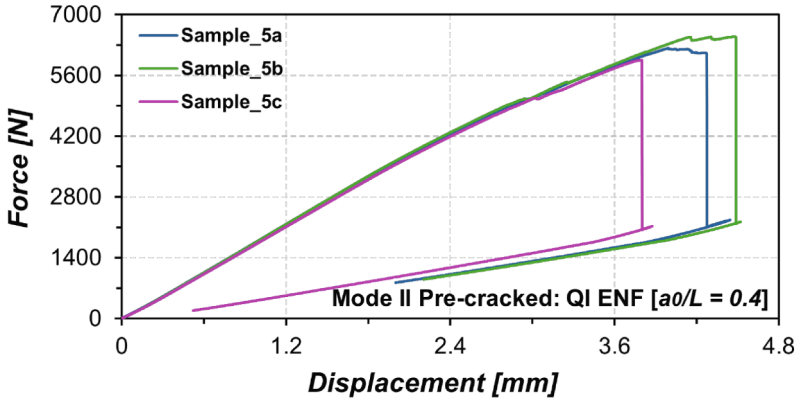

a

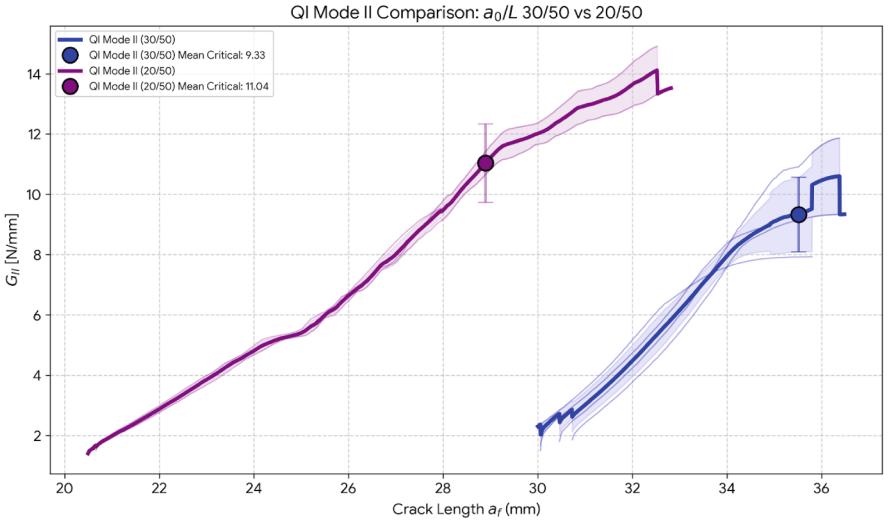

b

Fig. 8. (a) Force-Displacement graph of Mode II pre-cracked ENF QI specimens [a_0/L = 0.4; 20/50], (b) Variation of SERR vs. crack length for Mode II pre-cracked ENF QI specimens [a_0/L = 0.6 vs. 0.4; 30/50 vs. 20/50].

The above phenomena can be clearly understood by a mechanistic interpretation of the crack growth (Fig. 9). This shift in behavior is due to the stress distribution associated with the larger available bond-line space. In the specimens with an a_0/L ratio of *0.4*, the FPZ is large, and the crack growth remains less tortuous within the adhesive. However, as the specimen undergoes significant flexural bending, the global shear stresses eventually exceed the interlaminar strength of the ± 45°/0° interface across a broad region, rather than at a localized point at the crack tip. This triggers a global delamination of the substrate rather than localized migration.

These findings demonstrate that the fracture mechanism and damage tolerance of bonded composite joints are deeply coupled with the normalized crack geometry. This underscores that, for complex geometries, the transition between stable cohesive growth, crack migration, independent delamination, and catastrophic substrate failure is a function of FPZ evolution and differences in interlaminar strength between the laminate and the adhesive.

3.4. *Effect of span length on damage tolerance*

The absolute dimensions of the ENF specimens were increased while maintaining a constant normalized crack length ($a_0/L = 0.6$), to evaluate the scalability of the observed fracture mechanisms. The span length (*2 L*) was increased from 100 mm to 140 mm, corresponding to an increase in the initial delamination (a_0) from 30 mm to 42 mm. This geometric scaling was intended to account for the increased compliance and to determine if the crack migration behavior is a function of absolute specimen size or relative geometric ratios.

The specimens with the larger span exhibited an average failure load of 3771.3 ± 132.37 N, corresponding to a G_{IIC} of 9.41 ± 0.91 N/mm. Notably, this fracture toughness value is nearly identical to the G_{IIC} recorded for the specimens with a smaller span length but with the same a_0/L ratio (Fig. 10). The marginal difference (1% <) between the standard and large span length specimens validates that the fracture mechanism is independent of absolute span length when the normalized crack geometry is preserved. The increased span length resulted in higher compliance and, consequently, a lower peak load; the critical energy release rate remained constant. The consistency in G_{IIC} of the ENF specimens, with larger span lengths compared to smaller span lengths, and the same normalized crack geometry, can also be understood in terms of the stability of the FPZ and the invariance of the failure mechanism. Despite the change in absolute dimensions, the identical Mode II pre-cracking and constant normalized crack geometry produced an equivalent stress field at the crack tip (Fig. 11).

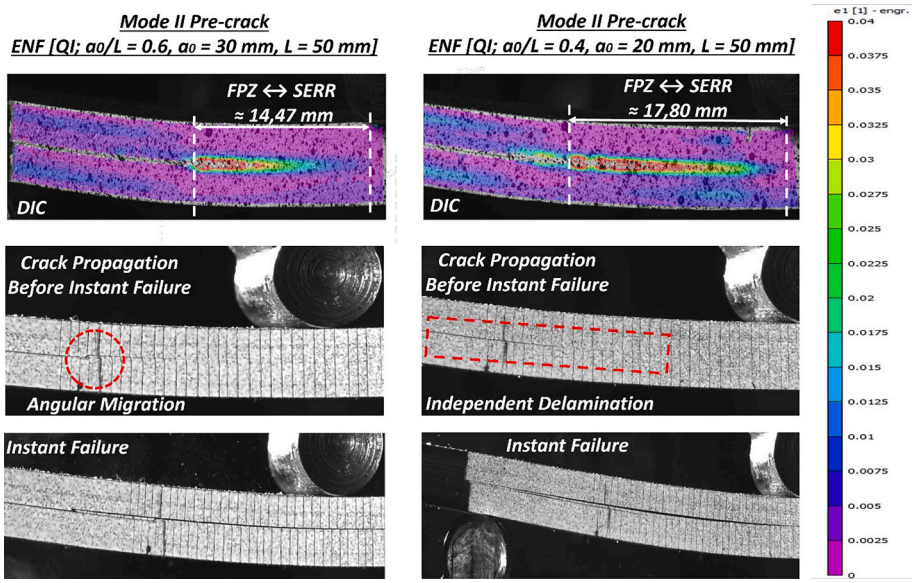

Fig. 9. DIC images coupled with camera car images showing qualitative FPZ evolution and morphology for Mode II pre-cracked ENF QI specimens [$a_0/L = 0.6$ vs. 0.4; 30/50 vs. 20/50].

Hence, an identical FPZ evolution was generated because the available space for the FPZ to evolve within the adhesive layer remained proportionally the same, resulting in a consistent energy dissipation capacity. Moreover, a consistent crack path was observed, as both small and large span specimens promoted crack migration at a characteristic angle of approximately 45°, transitioning from the adhesive bond layer into the weak interlaminar region of the laminates.

These results establish that the Mode II fracture characterization and crack migration mechanisms are governed by the normalized crack geometry rather than the absolute span length. This finding demonstrates significant practical importance, as the fracture analytics concluded from standard small-scale specimens can be reliably scaled to larger bonded structures, provided the a_0/L ratio and pre-cracking history are preserved.

3.5. Discussion

The primary damage mechanisms observed in the investigated systems include:

a) plastic deformation within the toughened adhesive layer (AF163-2 K)
b) micro-cracking and void growth within the FPZ
c) interlaminar delamination within the composite substrate, particularly in the QI laminates

Such interaction between adhesive plasticity and substrate delamination has also been reported in the literature for bonded composite systems [1,13,33,60,63–65]. The interaction between these damage modes was assessed by analyzing FPZ morphology and observing crack migration behavior.

In UD laminates, damage is confined to the adhesive layer, where interaction occurs between localized plastic deformation and shear-driven micro-damage ahead of the crack tip.

In contrast, for QI laminates, a more complex interaction is observed between the adhesive FPZ and the composite substrate's interlaminar strength. When the energy required to further develop the adhesive FPZ exceeds the interlaminar fracture resistance of critical interfaces (e.g., 45°/0°), crack migration from the adhesive layer into the composite substrate is triggered. This behavior reflects a direct interaction between adhesive plasticity and substrate delamination mechanisms.

Furthermore, the CBBM, which employs an equivalent crack-length approach, inherently accounts for the combined effects of multiple energy-dissipation mechanisms [47,52]. In the presence of a sizable FPZ, the measured fracture toughness should be interpreted as an apparent or effective value, which incorporates both elastic and inelastic dissipation mechanisms. Equivalent or apparent crack length approaches (e.g., CBBM) account for this by embedding the nonlinear FPZ contribution into an effective elastic crack length. As a result, the interaction between different damage processes is implicitly captured through their collective influence on the global compliance response. It is noted that, unlike MMB-based approaches where mode partitioning may influence FPZ interpretation, the present ENF-based analysis enables a direct assessment of shear-dominated fracture mechanisms [34]. Fig. 12 schematically represents the interactions between failure mechanisms, pre-cracking mode, lay-up and geometry discussed in this section.

4. Conclusions

This study systematically evaluates the role of pre-cracking, laminate stacking sequence, and geometric ratio on the pure Mode II fracture characterization of adhesively bonded composite joints. The following conclusions are drawn:

- The fracture resistance and damage tolerance of bonded composite laminates are highly process-dependent and significantly influenced by the mode of pre-cracking. For UD adherends, where interlaminar strength is high, stable crack growth was observed regardless of the mode of pre-cracking. Here, Mode I pre-cracking captures the upper-bound fracture resistance by forcing a localized crack tip to dissipate extra energy during its transition to a shear-dominant state. On the contrary, mode II pre-crack specimens induce a broader FPZ that distributes damage ahead of the crack tip, thereby reducing the localized energy release rate at the crack tip and yielding a lower fracture toughness estimate. The results revealed a significant disparity in fracture toughness; the G_{IIC} value for Mode I pre-cracked UD ENF specimens was $\approx 14.67 \pm 0.99$ N/mm, whereas the Mode II pre-cracked UD ENF specimens displayed a lower G_{IIC} value of $\approx 11.85 \pm 0.87$ N/mm.
- A significant finding was the inversion of the G_{IIC} trend between UD and QI laminates. While Mode I pre-cracking yields higher toughness in UD, it triggers premature crack migration in QI laminates due to

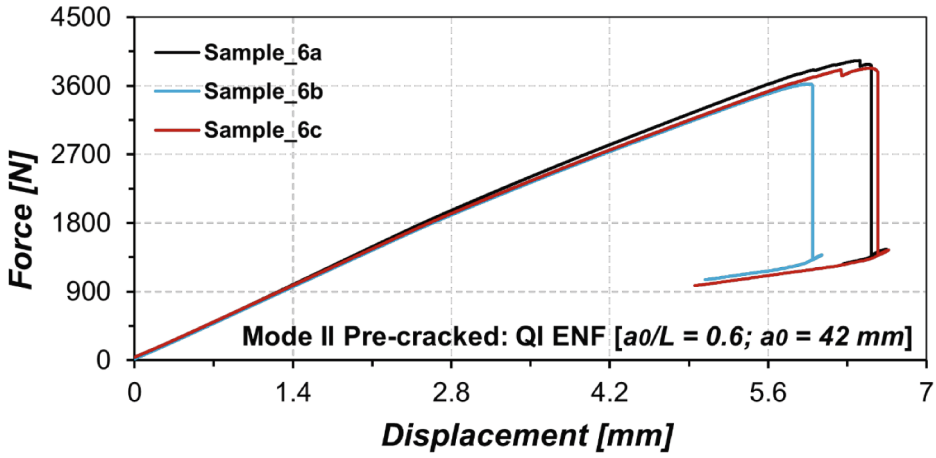

a

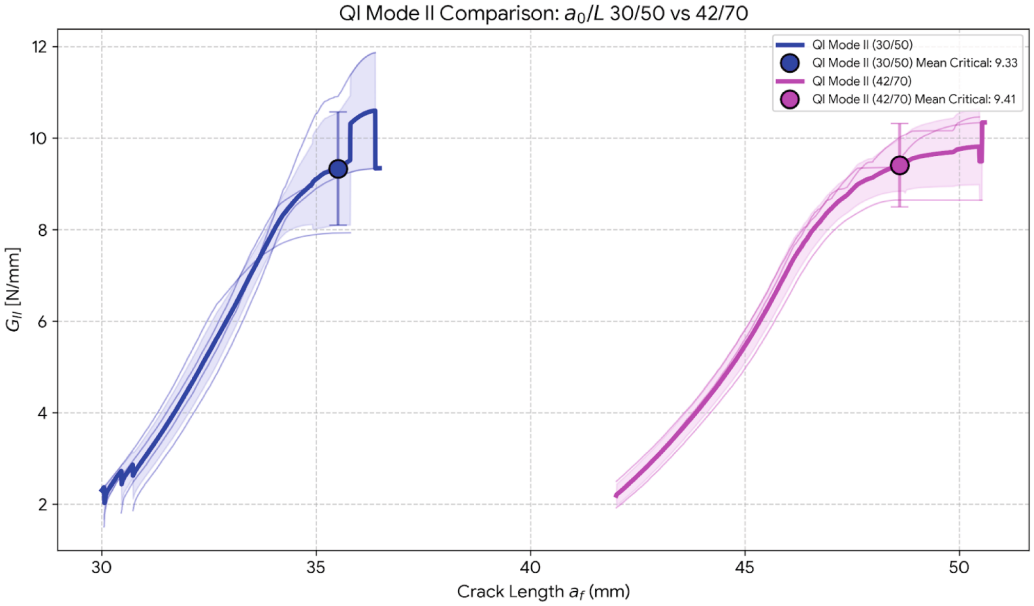

b

Fig. 10. (a) Force-Displacement graph of Mode II pre-cracked ENF QI specimens [a_0/L = 0.6; 42/70], (b) Variation of SERR vs. crack length for Mode II pre-cracked ENF QI specimens [a_0/L = 0.6; 30/50 vs. 42/70].

the high energy barrier required to expand a localized tip within the bond-layer relative to the weak interlaminar strength of the substrate. In QI laminates, mode II pre-cracking generates a broad, diffuse FPZ which acts as a mechanical buffer, stabilizing the crack within the adhesive layer and delaying migration into the composite substrate. As a result, the Mode II pre-cracked QI ENF specimens had a mean G_{IIC} of ≈ 9.33 ± 1.74 N/mm. In contrast, the Mode I pre-cracked QI ENF specimen displayed a reduced G_{IIC} of ≈ 7.31 ± 0.39 N/mm.

- The failure mechanism is highly sensitive to the normalized crack length. A shorter a_0/L ratio facilitates stable cohesive growth, followed by a sudden, two-sided independent delamination, whereas a longer a_0/L ratio promotes characteristic 45° angular crack migration. This underscores that for complex geometries, the transition between stable cohesive growth, crack migration, independent delamination, and catastrophic substrate failure is a function of the FPZ evolution and the differences in interlaminar strength between the laminate and the adhesive.
- Experimental results demonstrate that G_{IIC} and the associated crack migration mechanisms are independent of absolute span length, provided the a_0/L ratio and pre-cracking mode are held constant. This signifies a reliable scaling law for transitioning standard small-scale specimen data to large-scale applications.

The findings underscore that fracture resistance, crack growth mechanism, and damage tolerance in adhesively bonded composite joints are significantly influenced by process parameters.

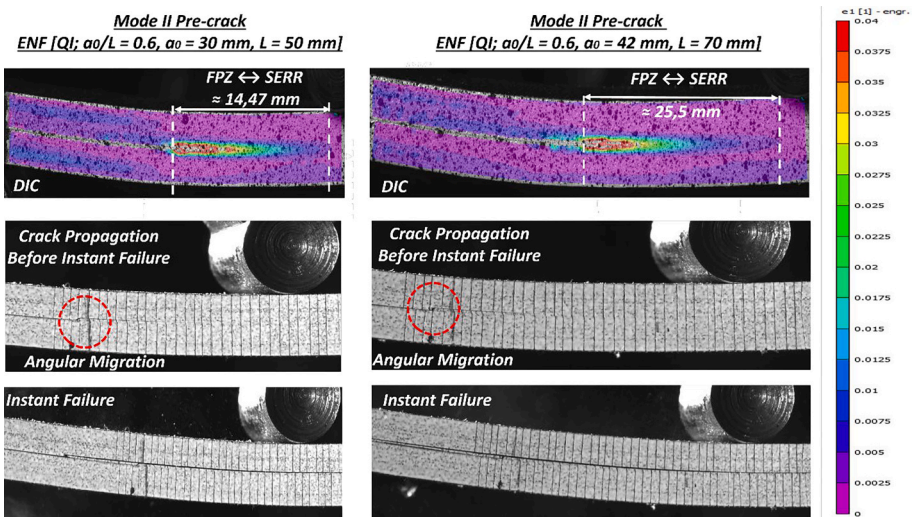

Fig. 11. DIC images coupled with camera car images showing qualitative FPZ evolution and morphology for Mode II pre-cracked ENF QI specimens [$a_0/L = 0.6$; 30/50 vs. 42/70].

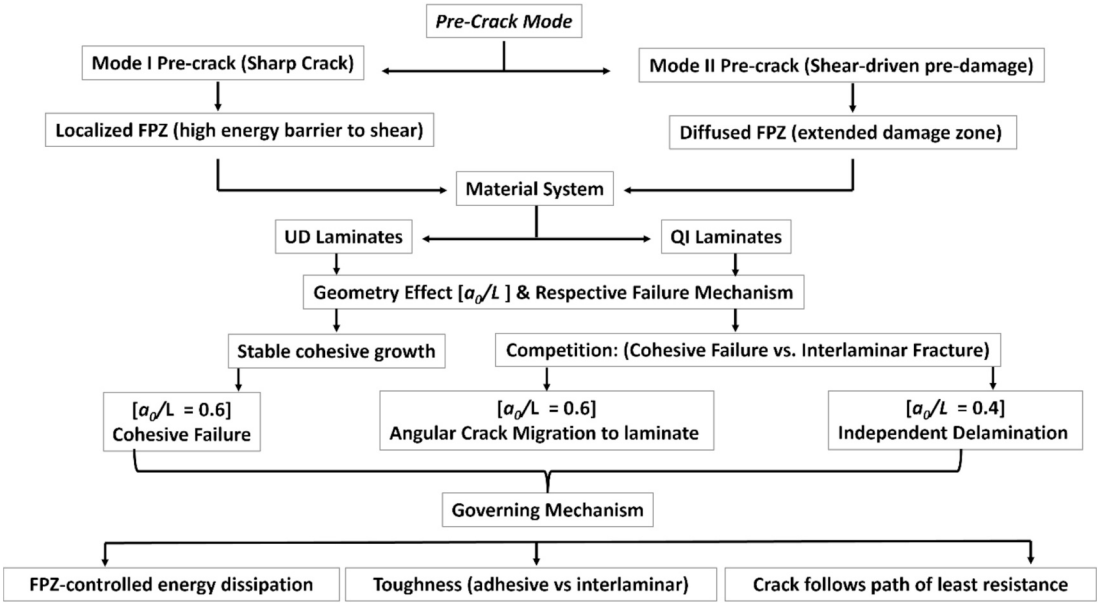

Fig. 12. Schematic flow diagram summarizing the relationships between pre-cracking conditions, FPZ evolution, and Mode II fracture characterization, providing an integrated overview of the key findings discussed in the study.

CRediT authorship contribution statement

Ishan Manoj: Writing – original draft, Visualization, Validation, Methodology, Investigation, Formal analysis, Data curation, Conceptualization. **Daniel Bernardes de Castro:** Validation, Investigation, Formal analysis, Data curation. **John-Alan Pascoe:** Writing – review & editing, Visualization, Supervision, Resources, Methodology, Funding acquisition, Conceptualization. **René Alderliesten:** Writing – review & editing, Visualization, Supervision, Resources, Methodology, Funding acquisition, Conceptualization.

Declaration of competing interest

The authors declare that they have no known competing financial interests or personal relationships that could have appeared to influence the work reported in this paper.

Acknowledgement

The project was carried out with a subsidy from the TSH Aircraft Manufacturing scheme of the Ministry of Economic Affairs, implemented by the Netherlands Enterprise Agency (RVO).

Data availability

Data will be made available on request.

References

[1] Pascoe JA. Fracture and Failure of Adhesives. Comprehensive Structural Integrity, Elsevier; 2023, p. V7-2-V7-23. https://doi.org/10.1016/B978-0-12-822944-6.00042-6.
[2] Jeevi G, Nayak SK, Abdul KM. Review on adhesive joints and their application in hybrid composite structures. J Adhes Sci Technol 2019;33:1497–520. https://doi.org/10.1080/01694243.2018.1543528.

[3] Manoj I, Jain A. Fracture behavior and strength enhancement of 3D-printed stepped-lap bonded joints using geometrically graded interfaces: experimental validation and damage modelling. J Adhes Sci Technol 2025:1–31. https://doi.org/10.1080/01694243.2025.2575812.

[4] Pascoe JA, Alderliesten RC, Benedictus R. On the relationship between disbond growth and the release of strain energy. Eng Fract Mech 2015;133:1–13. https://doi.org/10.1016/j.engfracmech.2014.10.027.

[5] Pascoe JA, Alderliesten RC, Benedictus R. Methods for the prediction of fatigue delamination growth in composites and adhesive bonds - a critical review. Eng Fract Mech 2013;112–113:72–96. https://doi.org/10.1016/j.engfracmech.2013.10.003.

[6] Chaves FJP, Da Silva LFM, De Moura MFSF, Dillard DA, Esteves VHC. Fracture mechanics tests in adhesively bonded joints: a literature review. J Adhes 2014;90:955–92. https://doi.org/10.1080/00218464.2013.859075.

[7] C das Neves PJ, M da Silva LF, Adams RD. Analysis of Mixed Adhesive Bonded Joints Part I: Theoretical Formulation. J Adhes Sci Technol 2009;23:1–34. DOI: 10.1163/156856108X336026.

[8] da Silva LFM, das Neves PJC, Adams RD, Spelt JK. Analytical models of adhesively bonded joints—Part I: Literature survey. Int J Adhes Adhes 2009;29:319–30. DOI: 10.1016/J.IJADHADH.2008.06.005.

[9] Pérez-Galmés M, Renart J, Sarrado C, Brunner AJ, Rodríguez-Bellido A. Towards a consensus on mode II adhesive fracture testing: Experimental study. Theor Appl Fract Mech 2018;98:210–9. https://doi.org/10.1016/j.tafmec.2018.09.014.

[10] Reis JP, de Moura MFSF, Moreira RDF. Extension of the crack equivalent method applied to mode II fracture of thermoplastic composites bonded joints using the ENF test. Compos Struct 2025;352. https://doi.org/10.1016/j.compstruct.2024.118687.

[11] Sun F, Lißner M, Petrinic N, Blackman BRK. Universal slope-based J-integral methods for characterization of the mode I, mode II and mixed mode I/II fracture behaviour of adhesively bonded interfaces. Compos Sci Technol 2024;252. https://doi.org/10.1016/j.compscitech.2024.110611.

[12] Sun F, Wang Q, Blackman BRK. Validity of LEFM to measure the Mode II and mixed Mode I/II fracture toughness of adhesively bonded CFRP. Compos A Appl Sci Manuf 2025;192. https://doi.org/10.1016/j.compositesa.2025.108777.

[13] Kupski J, Teixeira de Freitas S. Design of adhesively bonded lap joints with laminated CFRP adherends: Review, challenges and new opportunities for aerospace structures. Compos Struct 2021;268. https://doi.org/10.1016/j.compstruct.2021.113923.

[14] Test Method for Mixed Mode I-Mode II Interlaminar Fracture Toughness of Unidirectional Fiber Reinforced Polymer Matrix Composites 2022. DOI: 10.1520/D6671_D6671M-22.

[15] Fibre-reinforced plastic composites — Determination of the mode II fracture resistance for unidirectionally reinforced materials using the calibrated end-loaded split (C-ELS) test and an effective crack length approach ISO 15114.

[16] Blackman BRK, Kinloch AJ, Paraschi M. The determination of the mode II adhesive fracture resistance, GIIC, of structural adhesive joints: an effective crack length approach. Eng Fract Mech 2005;72:877–97. https://doi.org/10.1016/j.engfracmech.2004.08.007.

[17] Blackman BRK, Brunner AJ, Williams JG. Mode II fracture testing of composites: a new look at an old problem. Eng Fract Mech 2006;73:2443–55. https://doi.org/10.1016/j.engfracmech.2006.05.022.

[18] Iso 25217,. Adhesives - determination of the mode 1 adhesive fracture energy of structural adhesive joints using double cantilever beam and tapered double cantilever beam specimens. International Organization for Standardization: Standard; 2009.

[19] Demiral M, Kadioglu F. Failure behaviour of the adhesive layer and angle ply composite adherends in single lap joints: a numerical study. Int J Adhes Adhes 2018;87:181–90. https://doi.org/10.1016/j.ijadhadh.2018.10.010.

[20] Kadioglu F, Demiral M. Failure behaviour of the single lap joints of angle-plied composites under three point bending tests. J Adhes Sci Technol 2020;34:531–48. https://doi.org/10.1080/01694243.2019.1674101.

[21] Quan D, Wang G, Zhao G, Alderliesten R. On the fracture behaviour of aerospace-grade Polyether-ether-ketone composite-to-aluminium adhesive joints. Compos Commun 2022;30. https://doi.org/10.1016/j.coco.2022.101098.

[22] Carbas RJC, Marques EAS, da Silva LFM. The influence of epoxy adhesive toughness on the strength of hybrid laminate adhesive joints. Appl Adhes Sci 2021;9. https://doi.org/10.1186/s40563-020-00132-5.

[23] Morgado MA, Carbas RJC, dos Santos DG, da Silva LFM. Strength of CFRP joints reinforced with adhesive layers. Int J Adhes Adhes 2020;97. https://doi.org/10.1016/j.ijadhadh.2019.102475.

[24] Ramezani F, Nunes PDP, Carbas RJC, Marques EAS, da Silva LFM. The joint strength of hybrid composite joints reinforced with different laminates materials. Journal of Advanced Joining Processes 2022;5. https://doi.org/10.1016/j.jajp.2022.100103.

[25] Oshima S, Mikami T, Yoshimura A, Hirano Y, Ogasawara T. In situ optical observation of damage and failure process in adhesively bonded CFRP joints under mixed-mode loading. Compos Struct 2023;305. https://doi.org/10.1016/j.compstruct.2022.116453.

[26] Abylkassimov A, Kalimuldina G, Araby S, Amanbek Y. Failure mechanism investigation of the adhesively bonded joints using Finite Element and Discrete Element methods. Compos Struct 2025;351. https://doi.org/10.1016/j.compstruct.2024.118574.

[27] Ebrahimi MT, Khaji Z, Fakoor M. On mixed-mode fracture of brittle orthotropic solids: a novel micromechanical damage model. Eng Fract Mech 2025;313. https://doi.org/10.1016/j.engfracmech.2024.110628.

[28] Fernlund G, Spelt JK. Mixed-mode fracture adhesive characterization of joints. vol. 50. 1994.

[29] Lima RAA, Tao R, Bernasconi A, Carboni M, Carrere N, Teixeira de Freitas S. Uncovering the toughening mechanisms of bonded joints through tailored CFRP layup. Compos B Eng 2023;263. https://doi.org/10.1016/j.compositesb.2023.110853.

[30] Morgado MA, Carbas RJC, Marques EAS, da Silva LFM. Reinforcement of CFRP single lap joints using metal laminates. Compos Struct 2019;230. https://doi.org/10.1016/j.compstruct.2019.111492.

[31] Sarrado C, Turon A, Renart J, Costa J. An experimental data reduction method for the mixed Mode Bending test based on the J-integral approach. Compos Sci Technol 2015;117:85–91. https://doi.org/10.1016/j.compscitech.2015.05.021.

[32] Sarrado C, Turon A, Costa J, Renart J. On the validity of linear elastic fracture mechanics methods to measure the fracture toughness of adhesive joints. Int J Solids Struct 2016;81:110–6. https://doi.org/10.1016/j.ijsolstr.2015.11.016.

[33] Birnie J, Biagini D, Falaschetti MP, Monticeli F, Pascoe J-A, Troiani E. Influence of R-ratio and fracture process zone development on mode II fatigue delamination 2026. https://doi.org/10.5281/zenodo.1.

[34] Manoj I, de Castro DB, Pascoe J-A, Alderliesten R. How differences in fracture process zone behavior prevent transferability of mixed-mode fracture toughness measurements in toughened adhesive CFRP joints. Theor Appl Fract Mech 2026;145:105617. https://doi.org/10.1016/j.tafmec.2026.105617.

[35] Davies P. Influence of ENF Specimen Geometry and Friction on the Mode II Delamination Resistance of Carbon/PEEK. J Thermoplast Compos Mater 1997;10:353–61. https://doi.org/10.1177/089270579701000404.

[36] Davies P, Sims GD, Blackman BRK, Brunner AJ, Kageyama K, Hojo M, et al. Comparison of test configurations for determination of mode II interlaminar fracture toughness results from international collaborative test programme. Plast, Rubber Compos 1999;28:432–7. https://doi.org/10.1179/146580199101540600.

[37] Toolabi M, Blackman BRK. Guidelines for selecting the dimensions of adhesively bonded end-loaded split joints: an approach based on numerical cohesive zone length. Eng Fract Mech 2018;203:250–65. https://doi.org/10.1016/j.engfracmech.2018.05.019.

[38] Liu H (Hannah), Qi G, Renaud G, Li G, Li C (Lucy). Application of the effective crack length method to model delamination of unidirectional composite laminates under Mode II shear loadings. Composites Part C: Open Access 2023;12. DOI: 10.1016/j.jcomc.2023.100401.

[39] Moore DR, Pavan A, Williams JG, Fracture E. Mechanics Testing Methods for Polymers, Adhesives and Composites. European Structural Integrity Society 2001;28:3–375.

[40] Yan X, Guo X, Gao Y, Lin Y, Zhang N, Zhao Q. Mode-II fracture toughness and crack propagation of pultruded carbon Fiber-Epoxy composites. Eng Fract Mech 2023;279. https://doi.org/10.1016/j.engfracmech.2022.109042.

[41] Paul A, Xu X, Shimizu T, Wisnom MR. The role of broken fibres on crack migration into 0° surface plies in adhesively bonded carbon fibre composite joints. Compos Struct 2021;276. https://doi.org/10.1016/j.compstruct.2021.114530.

[42] Salamat-Talab M, Kazemi H, Mahdavi M. Influence of yarn bundle orientation and areal density on the interlaminar fracture toughness of ENF composites. Eng Fract Mech 2025;315. https://doi.org/10.1016/j.engfracmech.2025.110806.

[43] Gfrerrer M, Koss V, Wiener J, Schuecker C, Brunner AJ, Pinter G. Comparing Mode I, Mode II and Mixed-Mode I/II interlaminar fracture toughness of glass and carbon fiber reinforced polymer laminates with the same epoxy matrix system. Eng Fract Mech 2025;320. https://doi.org/10.1016/j.engfracmech.2025.111009.

[44] Akbolat MÇ, Katnam KB, Soutis C, Potluri P, Sprenger S, Taylor J. On mode-I and mode-II interlaminar crack migration and R-curves in carbon/epoxy laminates with hybrid toughening via core-shell rubber particles and thermoplastic micro-fibre veils. Compos B Eng 2022;238. https://doi.org/10.1016/j.compositesb.2022.109900.

[45] HexPLy 8552 Data Sheet. www.hexcel.com. Physical Properties. n.d.

[46] 3M Scotch-Weld Structural Adhesive Film AF 163-2. n.d.

[47] de Moura MFSF, Campilho RDSG, Gonçalves JPM. Pure mode II fracture characterization of composite bonded joints. Int J Solids Struct 2009;46:1589–95. https://doi.org/10.1016/j.ijsolstr.2008.12.001.

[48] Carlsson LA, Gillespie JW, Pipes RB. On the Analysis and Design of the End Notched Flexure (ENF) Specimen for Mode II Testing. J Compos Mater 1986;20:594–604. https://doi.org/10.1177/002199838602000606.

[49] Mehrabi M, Martulli LM, Bernasconi A, Carboni M. Estimating crack tip position in adhesively bonded joints subjected to mode II quasi-static loading. Fatigue Fract Eng Mater Struct 2024;47:1262–80. https://doi.org/10.1111/ffe.14237.

[50] Wang Y, Williams JG. Corrections for Mode II fracture toughness specimens of composites materials. vol. 43. 1992.

[51] Blackman B, Sun F, Teixeira de Freitas S, de Barros S, Moreira Arouche M, Ivankovic A. Understanding fracture mode-mixity and its effects on bond performance. Advances in Structural Adhesive Bonding, Second Edition, Elsevier 2023:579–613. https://doi.org/10.1016/B978-0-323-91214-3.00015-6.

[52] de Moura MFSF, de Morais AB. Equivalent crack based analyses of ENF and ELS tests. Eng Fract Mech 2008;75:2584–96. https://doi.org/10.1016/j.engfracmech.2007.03.005.

[53] de Moura MFSF, Silva MAL, de Morais AB, Morais JJL. Equivalent crack based mode II fracture characterization of wood. Eng Fract Mech 2006;73:978–93. https://doi.org/10.1016/j.engfracmech.2006.01.004.

[54] Arouche MM, Pavlovic M. Experimental and numerical analysis of the effect of temperature on the mode I and mode II delamination of glass fiber woven composites. Compos B Eng 2025;293. https://doi.org/10.1016/j.compositesb.2025.112131.

[55] Zhao LC, Yuan L, Wang ZR. Influence of 3D printing parameters on the fracture behavior of adhesive joints under mode II quasi-static loading: experimental and numerical insights. J Adhes 2025. https://doi.org/10.1080/00218464.2025.2602654.
[56] De Baere I, Jacques S, Van Paepegem W, Degrieck J. Study of the mode i and mode II interlaminar behaviour of a carbon fabric reinforced thermoplastic. Polym Test 2012;31:322–32. https://doi.org/10.1016/j.polymertesting.2011.12.009.
[57] Brunner AJ. Experimental aspects of Mode I and Mode II fracture toughness testing of ®bre-reinforced polymer-matrix composites. n.d.
[58] Nairn JA, Aimene YE. A re-evaluation of mixed-mode cohesive zone modeling based on strength concepts instead of traction laws. Eng Fract Mech 2021;248. https://doi.org/10.1016/j.engfracmech.2021.107704.
[59] Ayatollahi MR, Ajdani A, Akhavan-Safar A, da Silva LFM. Effect of notch length and pre-crack size on mode II fracture energy of brittle adhesives. Eng Fract Mech 2019;212:123–35. https://doi.org/10.1016/j.engfracmech.2019.03.024.
[60] Pernice MF, De Carvalho NV, Ratcliffe JG, Hallett SR. Experimental study on delamination migration in composite laminates. Compos A Appl Sci Manuf 2015;73:20–34. https://doi.org/10.1016/j.compositesa.2015.02.018.
[61] Wanthal S, Schaefer J, Justusson B, Hyder I, Engelstad S, Rose C. Paper Number: Session Topic: Verification & Validation of Progressive Damage/Failure Analysis for Stiffened Composite Structures Title: Verification and Validation Process for Progressive Damage and Failure Analysis Methods in the NASA Advanced Composites Consortium. n.d.
[62] Dávila CG, Weeks S, Czabaj M. Propagation rate transients in J-controlled fatigue characterization of adhesives. Int J Fatigue 2024;185. https://doi.org/10.1016/j.ijfatigue.2024.108377.
[63] Budhe S, Banea MD, de Barros S, da Silva LFM. An updated review of adhesively bonded joints in composite materials. Int J Adhes Adhes 2017;72:30–42. https://doi.org/10.1016/j.ijadhadh.2016.10.010.
[64] Oshima S, Koyanagi J. Review on damage and failure in Adhesively Bonded Composite Joints: a Microscopic Aspect. Polymers (Basel) 2025;17. https://doi.org/10.3390/polym17030377.
[65] Manoj I, Jain A. International Journal of Adhesion and Adhesives Strength improvement and failure analysis of dissimilar FDM printed single-lap joints with tailored interface geometry. Int J Adhes Adhes 2025;136:103876. https://doi.org/10.1016/j.ijadhadh.2024.103876.